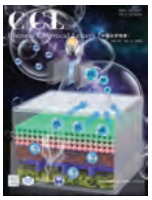
Chinese Chemical Letters 37 (2026) 111704

Contents lists available at ScienceDirect

Chinese Chemical Letters

journal homepage: www.elsevier.com/locate/cclet



A microfluidic biosensor for rapid detection of live bacteria based on immune magnetic separation and photothermal lysis of gold nanorods

Nan Li[a], Weifei Zhang[b], Gaowa Xing[b], Zengnan Wu[b], Xiaorui Wang[c], Ling Lin[c,*]

[a] School of Chinese Materia Medica, Beijing University of Chinese Medicine, Beijing 100029, China
[b] Department of Chemistry, Beijing Key Laboratory of Microanalytical Methods and Instrumentation, Key Laboratory of Bioorganic Phosphorus Chemistry and Chemical Biology (Ministry of Education), Tsinghua University, Beijing 100084, China
[c] Department of Bioengineering, Beijing Technology and Business University, Beijing 100048, China

ARTICLE INFO

Article history:
Received 11 April 2025
Revised 12 July 2025
Accepted 10 August 2025
Available online 11 August 2025

Keywords:
Microfluidic biosensors
Live bacteria detection
Immune magnetic separation
Photothermal lysis
ATP bioluminescence

ABSTRACT

Foodborne bacterial infection is a serious threat to food safety, especially live pathogens causing outbreaks of most diseases. Thus developing live bacterial detection methods is important for public health. In this study, a microfluidic biosensor was developed for rapid detection of live *Salmonella typhimurium*, in which immune magnetic particle chains in microchannels were used to separate and enrich target bacteria, antibody-conjugated gold nanorods (GNRs) were applied for photothermal lysis of target live bacteria under near-infrared (NIR) irradiation, and a photon-counting detector was used for measuring adenosine triphosphate (ATP) bioluminescence in the presence of firefly luciferin/luciferase. This biosensor was proved to be able to quantitatively detect *S. typhimurium* from 5.0×10^2 CFU/mL to 5.0×10^6 CFU/mL in 60 min (magnetic separation 20 min; GNRs combination 20 min; NIR irradiation, 8 min) with limit of detection (LOD) of 495 CFU/mL. This biosensor showed an excellent specificity in the coexistence of other foodborne bacteria, and target bacteria were successfully measured even in the matrix interference of milk sample with mean recovery of 121.17 %. This biosensor might be a promising tool for on-site assessment foodborne bacteria.

© 2026 Published by Elsevier B.V. on behalf of Chinese Chemical Society and Institute of Materia Medica, Chinese Academy of Medical Sciences.

Foodborne pathogens have been recognized as a worldwide concern about food safety and public health [1,2]. Since most diseases are caused by live pathogens, developing rapid and sensitive methods to measure live bacteria is in high demand [3–5]. The gold standard method for live bacterial detection is colony-counting, but this approach requires several days for bacterial cultivation, which delays the result readout [6]. Nucleic acid-based molecular detection approaches [7–9], aptamer-based recognition strategies [10–12], and immunological methods [13–15] are widely used to identify and detect specific bacteria within a few hours, but these methods cannot effectively distinguish live bacteria from dead bacteria, which will result in false positive results and interfere with the correct assessment of food safety risks by regulatory authorities. In contrast, adenosine triphosphate (ATP)-based bioluminescence methods can specifically and rapidly detect live bacteria *via* firefly luciferin/luciferase reaction [16,17]. This method is widely used in the detection of bacterial contamination on food and environmental surfaces. However, such methods are not specific and cannot differentiate between different pathogenic bacteria. Therefore, there is an urgent demand to develop some rapid approaches for the detection of live specific bacteria.

Recently, gold nanorods (GNRs) have been applied to rupture the bacteria owing to the advantages of photothermal effect [18,19]. GNRs can be regulated to absorb near-infrared (NIR) radiation according to their size and shape, and the radiation energy can be transformed into heat [18]. Given this characteristic, if antibody-conjugated GNRs can specifically adhere to the target bacterial surface, the localized heat generated during NIR irradiation would cause target bacterial lysis [20]. Although this strategy can selectively kill or destroy the target bacteria, it is incapable of quantitative bacterial detection. To this end, combining GNRs-targeted photothermal lysis of bacteria with ATP-based bioluminescence measure becomes promising for the detection of specific live bacteria [21].

Food samples usually have complex matrix interference, and the target bacterial concentration is generally low, in consequence, the specific separation of target bacteria plays an important role in rapid and sensitive detection of foodborne pathogens [22,23]. The immunomagnetic separation method has been considered as a crucial technique for sample pretreatment in the past decade [24,25].

* Corresponding author.
E-mail address: linling@btbu.edu.cn (L. Lin).

https://doi.org/10.1016/j.cclet.2025.111704
1001-8417/© 2026 Published by Elsevier B.V. on behalf of Chinese Chemical Society and Institute of Materia Medica, Chinese Academy of Medical Sciences.

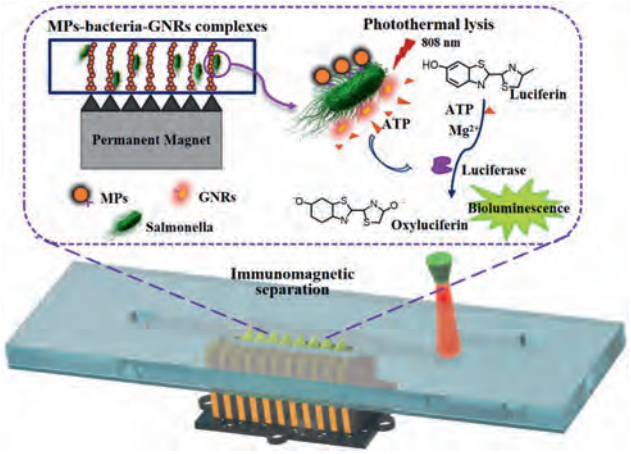


Fig. 1. Schematic of this microfluidic biosensor for rapid detection of live *Salmonella typhimurium* based on immune magnetic separation and photothermal lysis of gold nanorods.

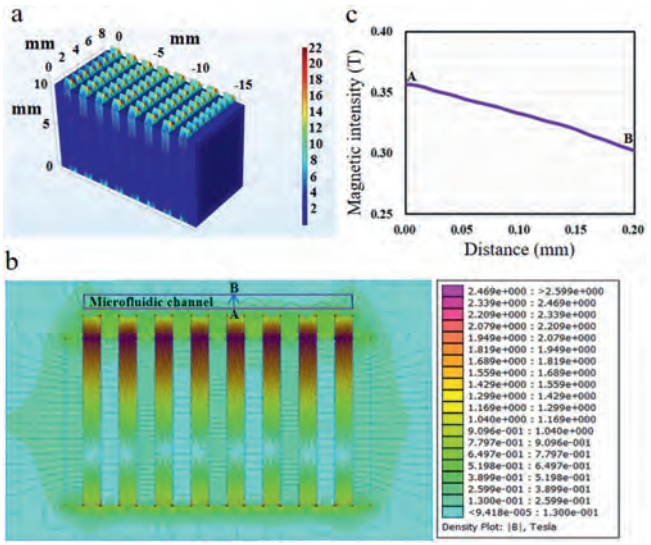


Fig. 2. Analysis of the high gradient magnetic field. (a) Simulation of the magnetic fields using COMSOL software. (b) The distribution of the magnetic field in microfluidic channel simulated with FEMM software. (c) The change of magnetic intensity with the channel height.

Conventional methods for immunomagnetic separation are usually performed in centrifuge tubes, which can only process small sample volumes due to the limited spatial distance of the magnetic field [26,27]. The microfluidic devices allow continuous-flow separation of target pathogens in the microchannel, greatly increasing the volume of the processed sample and improving the detection sensitivity [28,29]. Additionally, in order to reduce the consumption of magnetic particles (MPs) and ensure sufficient contact between pathogens and immune MPs, it is usually necessary to immobilize MPs as a chain or net structure in the microfluidic channel, which can significantly improve the separation efficiency of the target bacteria [30].

Herein, in this work, a microfluidic biosensor integrated with MP chains was developed for rapid detection of live foodborne pathogens based on ATP bioluminescent signals caused by antibody-conjugated GNRs photothermal lysis (Fig. 1), and the physical picture of microfluidic device was provided in Fig. S1 (Supporting information). A major foodborne pathogen, *S. typhimurium*, which commonly leads to serious emergencies, was used as target bacteria to demonstrate the feasibility of this biosensor. The immune MPs were first injected into the microfluidic channel. Since a high gradient magnetic field was installed under the microfluidic chip using mutual repelling permanent magnets separated by sawtooth-shaped iron slices, the MPs in microfluidic channels could form into chain structures at the tips of sawtooth. The magnetic field was simulated using the finite element analysis software COMSOL, as shown in Fig. 2a, a high gradient magnetic field was generated at each tip of the iron slices. To better understand the distribution of the magnetic field in microfluidic channels, the FEMM software was used to analyze the magnetic zone, as shown in Figs. 2b and c, an average magnetic intensity of ~0.33 T and a mean gradient of ~300 T/m was exhibited from the bottom of channel (A) to the top of channel (B). Then, the sample containing *S. typhimurium* was continuous-flow injected into the microfluidic channel, and the target bacteria were specifically captured on the MP chains modified with the capture anti-*S. typhimurium* antibodies (CAbs). Next, GNRs conjugated with detection anti-*S. typhimurium* antibodies (DAbs) were introduced into the microfluidic channel and incubated with the *S. typhimurium* to form the MPs-bacteria-GNRs complexes. Subsequently, the complexes were irradiated with NIR laser, and the photothermal effect of GNRs triggered *S. typhimurium* lysis and ATP release. The released ATP was monitored based on the bioluminescent signals *via* the firefly luciferin/luciferase reaction. Since each bacterium contained essentially the same ATP molecule, the signal intensity was proportional to the amount of lysed *S. typhimurium*. It should be noted, the dual antibody identification, including CAbs and DAbs, further enhanced the specificity of target detection.

To verify the successful modification of CAbs on MPs, the anti-*S. typhimurium* antibody-modified MPs were used to capture target bacteria in centrifuged tubes, after magnetic separation, the number of *S. typhimurium* in supernatant and MPs were counted using the conventional culture plating method, separately. As shown in Fig. S2a (Supporting information), almost all the bacteria were captured by immune MPs. Besides, to prove the credibility of the results, anti-*Escherichia coli* O157:H7 antibody-modified MPs were used to capture *S. typhimurium*, and the results exhibited few bacteria were attached on the MPs. The specificity of anti-*S. typhimurium* antibody-modified MPs was also explored by comparing the capture efficiency of different bacteria, as shown in Fig. S2b (Supporting information), the capture rate of *S. typhimurium* was as high as 90.83 %, in contrast, only 3.33 % *E. coli* O157:H7 was nonspecifically adsorbed on the immune MPs. These results verified the successful modification of CAbs on MPs. Further, transmission electron microscope (TEM) images showed the formation of MPs-*S. typhimurium*, demonstrating the capture performance of immune MPs (Fig. 3a). To demonstrate the successful conjugation of antibody on carboxyl-functionalized GNRs, the visible absorption spectra, zeta potential measurement and TEM images were investigated, separately. GNRs had two absorption peaks in visible spectra, including a transverse absorption peak at 510 nm and a longitudinal absorption peak at 810 nm. After antibody was conjugated on GRNs, a slight red shift of longitudinal absorption peak was observed (Fig. S3a in Supporting information). This was because the changes of GNRs size, shape and surface charge after antibody modification caused the selective absorption of visible light. Additionally, the zeta potential was measured to verify the conjugation formation. Carboxylated GNRs were electronegative in PBS buffer with −10.58 mV potential, and antibody was electropositive in PBS buffer, the results showed the potential of antibody-GNRs was −9.53 mV, confirming the formation of conjugation (Fig. S3b in Supporting information). TEM images exhibited the morphology of GNRs before and after modification, but no obvious difference was observed owing to the size of antibody in nano-scale (Fig. S3c in Supporting information). Further, different antibody-

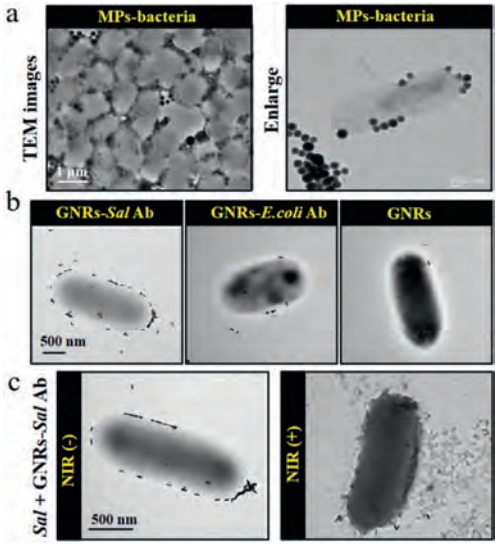


Fig. 3. TEM images of bacteria. (a) Anti-*Salmonella typhimurium* antibody-modified MPs adhered on *Salmonella typhimurium*. (b) Anti-*Salmonella typhimurium* antibody-conjugated GNRs adhered on *Salmonella typhimurium* (left), anti-*E. coli* O157:H7 antibody-conjugated GNRs (middle) and bare GNRs (right) nonspecifically adsorbed on *Salmonella typhimurium*. (c) Targeted photothermal lysis of *Salmonella typhimurium* by anti-*Salmonella typhimurium* antibody-conjugated GNRs in the presence (right) and absence (left) of NIR irradiation.

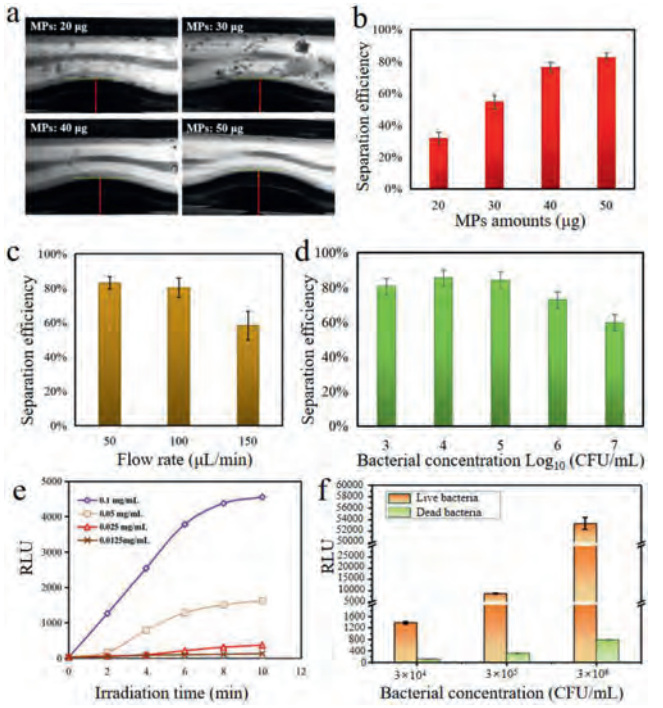


Fig. 4. Optimization of magnetic separation and photothermal lysis on this microfluidic biosensor. (a) Images of the dot-array magnetic particle chains using different amounts of MPs. (b) The change of separation efficiency with the amounts of MPs at a bacterial concentration of 10^4 CFU/mL with a flow rate of 50 μL/min. (c) The change of separation efficiency with the flow rate at a bacterial concentration of 10^4 CFU/mL with 50 μg MPs. (d) The separation efficiency at different bacterial concentrations with 50 μg MPs and 50 μL/min flow rate. (e) Bioluminescent signals generated from various concentrations of immune GNRs and different irradiation time. (f) The bioluminescent signals generated from live and dead *Salmonella typhimurium* after photothermal lysis.

modified GNRs were incubated with *Salmonella*, only anti-*S. typhimurium* antibody-conjugated GNRs fully adhered on the bacterial surface, while few anti-*E. coli* O157:H7 antibody-conjugated GNRs and bare GNRs were adsorbed on bacterial surface (Fig. 3b). To prove that photothermal effect of GNRs can cause bacterial lysis under NIR irradiation (808 nm), the lethal temperature of bacteria was first explored. As shown in Fig. S4a (Supporting information), when bacteria were heated at 65 °C for 10 min, the mortality rate could reach 80 %. Then, the photothermal effect of different concentrations GNRs in solution was monitored, as shown in Fig. S4b (Supporting information), the solution temperature was positively associated with GNRs concentration. When GNRs concentration was 0.1 mg/mL, the solution temperature increased to above 65 °C after 6 min of NIR laser irradiation, indicating that the photothermal effect of GNRs was able to cause bacterial lysis and death. Furthermore, antibody-modified GNRs were incubated with bacteria, and the bacterial morphology before and after NIR irradiation was observed *via* TEM imaging. As shown in Fig. 3c, the surface of bacteria without NIR irradiation was smooth with a complete bacterial structure; while the surface of bacteria after NIR irradiation was obviously damaged, verifying the photothermal lysis capability of antibody-modified GNRs.

Further, to optimize the magnetic separation efficiency of target bacteria, two key parameters including the amount of MPs and flow rate were investigated by calculating the ratio of bacteria on MPs to original bacteria. Firstly, the amount of MPs was optimized, different amounts of MPs (20, 30, 40, 50 μg) in PBS buffer were injected into the microfluidic channel to generate chain structures. As shown in Fig. 4a, the chain height was related to the amount of MPs, and an obvious chain structure was formed with 50 μg MPs. Meanwhile, the separation efficiency was improved from 31.69 % to 82.39 % when the amount of MPs was increased from 20 μg to 50 μg at a flow rate of 50 μL/min with 10^4 CFU/mL *S. typhimurium* (Fig. 4b), thus the amount of 50 μg was determined in the following experiments. Besides, the flow rate also had a great impact on the integrity of chain structures and the contact probability between the MPs and *S. typhimurium*. If the fluid flow rate was too fast, the chain structures would be destroyed, and at the same time, the collision and contact between MPs and *S. typhimurium* would be insufficient, thus affecting the separation efficiency. In contrast, if the flow rate was too slow, although the chain structure could remain intact, and the sufficient contact between MPs and target bacteria was allowed, it would make the target separation time too long, thus it was necessary to reasonably optimize the flow rate to balance the separation efficiency and time. To this end, the influence of flow rate on chain structural integrity was explored, and we found that chain structure kept intact when the flow rate was less than 150 μL/min, while when the flow rate was more than 200 μL/min, the chain structure began to be destroyed, accompanied by partial tilting and collapse. Hence, we focused on investigating the effect of three different flow rates (50, 100, 150 μL/min) on *S. typhimurium* separation efficiency with a bacterial concentration of 10^4 CFU/mL. As shown in Fig. 4c, a flow rate of 50 μL/min allowed a highest separation efficiency with a value of 83.2 % owing to the sufficient immune reaction time, thus a flow rate of 50 μL/min was determined in the following experiments. Based on the above optimization parameters, we further explored the separation efficiency of different concentrations of target bacteria. As shown in Fig. 4d, the separation efficiency of *S. typhimurium* with 10^3–10^5 CFU/mL was more than 80 %, while a lower separation efficiency was observed with a range from 10^6 to 10^7 CFU/mL. One possible reason might be that the limited binding sites and steric hindrance on MPs chain partly restrained the combination of high concentrations of bacteria. However, this would not be a concern because the concentration of target bacteria in practical samples was usually in a low range. To optimize the photothermal lysis efficiency of target bacteria, the antibody-conjugated GNRs were injected into the chan-

nel and incubated with *S. typhimurium* for 20 min to allow specific binding. The free GNRs were washed away, and a sandwich structure of MPs-*S. typhimurium*-GNRs was obtained. Although both the antibodies modified on MPs and GNRs could identify *S. typhimurium*, they targeted different epitopes on bacterial surface without mutual competition. More than that, two immune identification greatly improved the separation specificity and reduced the interference of non-target substances. Subsequently, the MPs-*S. typhimurium*-GNRs were irradiated by 808 nm NIR laser, which led to the bacterial lysis and ATP release, generating bioluminescent signal in the presence of firefly luciferin/luciferase. We found that the bioluminescent signals reached a maximum with an addition of 0.1 mg/mL antibody-conjugated GNRs, suggesting a sufficient immune reaction between GNRs and *S. typhimurium*. Further, given that photothermal effect was dependent upon NIR irradiation time, we investigated the change of bioluminescent signals with increasing irradiation time. The results showed irradiation within an 8 min period dramatically caused ATP release, whereas extended irradiation time (10 min) did not significantly increase bioluminescent signals (Fig. 4e). In addition, to demonstrate that this approach was able to specifically detect live *S. typhimurium* without the interference of dead bacteria, the bioluminescent signals generated from the same concentration of live *S. typhimurium* and dead *S. typhimurium* (inactivated at 70 °C for 10 min) were measured, respectively. As shown in Fig. 4f, after 8 min of NIR irradiation, the live *S. typhimurium* obviously generated strong bioluminescent signals, while the signal from dead *S. typhimurium* was extremely weak, indicating the method specificity for live *S. typhimurium*.

Having defined the above parameters, different concentrations of *S. typhimurium* ranging from 5×10^1 CFU/mL to 5×10^6 CFU/mL were detected to determine the calibration curve between bioluminescent signal (*RLU*) and bacterial concentration (*C*), and each concentration was repeated for three parallel tests. As shown in Fig. 5a, a good linear relationship was obtained from 5×10^2 CFU/mL to 5×10^6 CFU/mL, which was expressed as $\log_{10}(RLU) = 0.8\log_{10}(C) - 0.446$ ($R^2 = 0.998$). The LOD was defined as the analyte concentration giving a signal equal to the blank signal plus 3 × standard deviation (SD) of the blank, and the calculation result of LOD was 495 CFU/mL. Although the LOD of this biosensor showed a comparable sensitivity in contrast to most methods, it was not so impressive compared to some strategies using target amplification or signal amplification. Thus in our future work, for the further improvement of detection sensitivity, we would try to develop strategies for ATP signal amplification. The specificity of this microfluidic biosensor was evaluated by measuring three kinds of bacteria, including 10^4 CFU/mL target bacteria (*S. typhimurium*) and 10^6 CFU/mL nontarget bacteria (*E. coli* O157:H7 and *Staphylococcus aureus*). As shown in Fig. 5b, only *S. typhimurium* emitted strong signals, while the nontarget bacteria exhibited weak signals. Additionally, coexistence of *S. typhimurium* with other nontarget bacteria did not influence the signal. These results demonstrated that this microfluidic biosensor had a good specificity toward *S. typhimurium*, regardless of the presence of nontarget bacteria or other interferences.

The practical applicability of this microfluidic biosensor was verified by detecting different concentrations of *S. typhimurium* in spiked milk samples. The added bacterial concentration was counted by the gold standard culture method, and the detected bacterial concentration was calculated according to calibration curve between bioluminescent signals and bacterial concentration. As shown in Table S1 (Supporting information), the detected bioluminescent signal showed an upward trend with the increase of *S. typhimurium* concentration, however, we found that all the calculated *S. typhimurium* concentrations were higher than the actual added concentrations. We deduced there were two possible

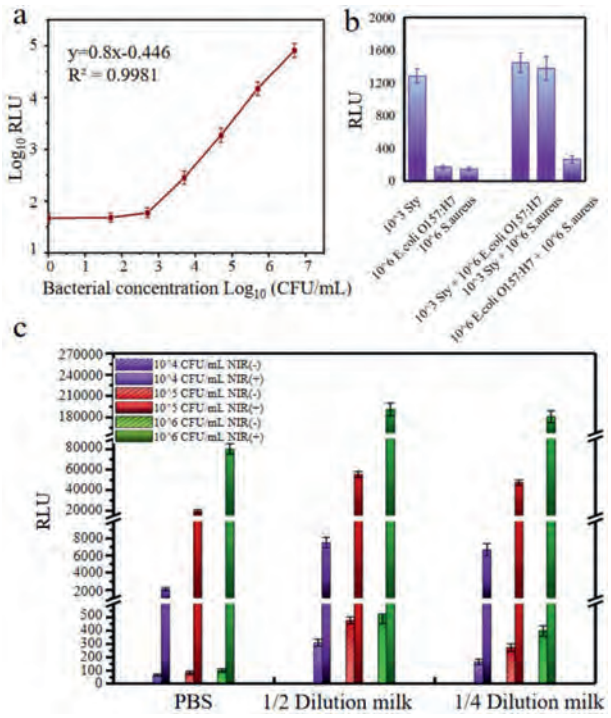


Fig. 5. Performance evaluation of this microfluidic biosensor. (a) Calibration curve of this biosensor for detection of *Salmonella typhimurium* at the concentrations of 5×10^2 CFU/mL to 5×10^6 CFU/mL ($n = 3$). (b) Specificity evaluation of this biosensor in the presence of interfering bacteria (*E. coli* O157:H7 *and Staphylococcus aureus*). (c) Bioluminescent signals generated from various concentrations of bacteria spiked in PBS and milk, separately. NIR(-) represented in the absence of NIR laser irradiation, indicating the signals came from interferences in milk matrix; NIR(+) represented in the presence of NIR laser irradiation, indicating the signals came from both the residual milk matrix and ATP released from bacteria.

reasons for this result: one was that the residual matrix of milk samples interfered the ATP measure even though a washing step was performed to rinse the milk sample. The other possible reason was that when preparing the spiked bacterial samples, the bacteria proliferated due to the rich nutrients in the milk matrix, resulting in a higher detection result. To this end, a set of experiments were designed to verify the above two guesses. Different concentrations of bacteria (10^4, 10^5, 10^6 CFU/mL) were spiked into PBS buffer, 1/2 diluted milk samples (volume ratio of milk to PBS: 1:1), and 1/4 diluted milk samples (volume ratio of milk to PBS 1:3) for 2 h incubation, followed by magnetic separation. Then, PBS buffer was injected into the microfluidic channels to wash away the milk matrix prior to adding immune GNRs. Subsequently, the MPs-*S. typhimurium*-GNRs complexes were directly mixed with luciferase and luciferin substrate without NIR irradiation. The bioluminescent signals were recorded as NIR(-), which were mainly caused by the interference from residual milk matrix. Besides, the same samples were also performed to suffer from NIR laser irradiation for 8 min, recorded as NIR(+), and these bioluminescent signals were caused by the combined effect of interference from residual milk matrix and ATP released from *S. typhimurium*. As shown in Fig. 5c, the signals of each group in NIR(+) were much stronger than those in NIR(-), suggesting that the residual matrix interference could be ignored. Therefore, a likely reason for the overestimated bacterial concentration might be that *S. typhimurium* multiplied greatly during the 2 h in milk. To prove this hypothesis, the number of detected bacteria in milk and PBS buffer was calculated, respectively. As shown in Table S2 (Supporting information), the number of bacteria in milk samples was much higher than that in PBS buffer for each group of bacterial concentration, indicating that the overestimated results were due to the bacterial proliferation.

In conclusion, in this study, a microfluidic biosensor integrated with immune magnetic separation was successfully developed for rapid detection of live *S. typhimurium* using ATP bioluminescence methods caused by specific photothermal lysis. The MP chains in microfluidic channels allowed the target separation and enrichment from large-volume milk samples. The photothermal effect of antibody-conjugated GNRs caused bacterial lysis accompanied by ATP release, making it possible to selectively detect live *S. typhimurium*. This biosensor effectively avoided the interference of false positives resulted from dead bacteria in the sample with the advantages of fast detection speed, strong sample processing ability, and high specificity, and was expected to be used as a promising tool for the rapid detection of live food-borne pathogens to ensure food safety.

Declaration of competing interest

The authors declare that they have no known competing financial interest or personal relationships that could have appeared to influence the work reported in this paper.

CRediT authorship contribution statement

Nan Li: Writing – original draft, Resources, Methodology, Funding acquisition, Formal analysis, Data curation. **Weifei Zhang:** Methodology, Investigation. **Gaowa Xing:** Investigation, Data curation. **Zengnan Wu:** Investigation, Data curation. **Xiaorui Wang:** Investigation, Data curation. **Ling Lin:** Writing – review & editing, Validation, Supervision, Funding acquisition.

Acknowledgments

This work was supported by the National Natural Science Foundation of China (Nos. 82404857, 22322401, 22204155), the Young Elite Scientists Sponsorship Program by CACM (No. 2023-QNRC2-B10), and the Fundamental Research Funds for the Central Universities (No. 2022-JYB-JBZR-018).

Supplementary materials

Supplementary material associated with this article can be found, in the online version, at doi:10.1016/j.cclet.2025.111704.

References

[1] N. Li, W. Zhang, J. Lin, et al., Anal. Chem. 94 (2022) 3963–3969.
[2] G. Xing, Y. Shang, J. Ai, et al., Anal. Chem. 95 (2023) 13391–13399.
[3] M. Calimci, T. Tezcan, E.K. Tayyarcan, et al., Talanta 286 (2025) 127569.
[4] W. Yin, K. Hu, Y. Yang, et al., Anal. Chem. 96 (2024) 17941–17949.
[5] X. Wang, X. Hu, S. Pan, et al., Sensor. Actuat. B: Chem. 408 (2024) 135543.
[6] G. Xing, W. Zhang, N. Li, Q. Pu, J.M. Lin, Chin. Chem. Lett. 33 (2022) 1743–1751.
[7] S. Wang, G. Cai, H. Duan, W. Qi, J. Lin, Lab Chip 22 (2022) 80–89.
[8] Y. Shang, J. Sun, Y. Ye, et al., Crit. Rev. Food Sci. Nutr. 60 (2020) 201–224.
[9] Y. Shang, G. Xing, J. Lin, et al., Biosens. Bioelectron. 243 (2024) 115771.
[10] M. Xiao, K. Zou, L. Li, et al., Angew. Chem. Int. Ed. 58 (2019) 15448–15454.
[11] M. Agar, M. Laabei, H.S. Leese, P. Estrela, Biosens. Bioelectron. 272 (2025) 117136.
[12] Y. Zhang, Y. Liu, Y. Yang, et al., Chin. Chem. Lett. 34 (2023) 108102.
[13] W. Qi, L. Zheng, Y. Hou, et al., Food Chem. 381 (2022) 131801.
[14] F. Huang, L. Xue, W. Qi, et al., Biosens. Bioelectron. 176 (2021) 112921.
[15] Y. Shang, G. Xing, H. Lin, et al., Anal. Chem. 95 (2023) 13368–13375.
[16] W. Lee, D. Kwon, B. Chung, et al., Anal. Chem. 86 (2014) 6683–6688.
[17] M.M. Calabretta, R. Álvarez-Diduk, E. Michelini, A. Roda, A. Merkoçi, Biosens. Bioelectron. 150 (2020) 111902.
[18] J. Zhang, Y. Feng, J. Mi, et al., J. Hazard. Mater. 342 (2018) 121–130.
[19] X. Zhang, S. Zhou, Y. He, et al., Anal. Chem. 96 (2024) 13971–13979.
[20] R.S. Norman, J.W. Stone, A. Gole, C.J. Murphy, T.L. Sabo-Attwood, Nano Lett. 8 (2008) 302–306.
[21] S.U. Kim, E.J. Jo, Y. Noh, et al., Anal. Chem. 90 (2018) 10171–10178.
[22] G. Cai, Y. Wang, Y. Zhang, L. Zheng, J. Lin, Chin. Chem. Lett. 34 (2023) 108059.
[23] X. Fu, J. Sun, R. Liang, et al., Trends Food Sci. Technol. 116 (2021) 115–129.
[24] L. Wang, J. Lin, TrAC, Trends Anal. Chem. 128 (2020) 115915.
[25] X. Liu, Z. Guo, Y. Qiao, et al., J. Adv. Res. 77 (2025) 257–264.
[26] S. Wang, T. Peng, Q. Meng, et al., Sensor. Actuat. B: Chem. 324 (2020) 128654.
[27] M.J. Hwang, A.S. Jang, D.K. Lim, Sensor. Actuat. B: Chem. 329 (2021) 129134.
[28] L. Xue, N. Jin, R. Guo, et al., ACS Sens. 6 (2021) 2883–2892.
[29] F. Yang, T. Wang, S. Wang, et al., Anal. Chem. 97 (2025) 7231–7241.
[30] L. Xue, R. Guo, F. Huang, et al., Biosens. Bioelectron. 173 (2021) 112800.